



HAL
open science

Investigating the electrocatalytic oxidation of glycerol on simultaneous nitrogen- and fluorine-doped on activated carbon black composite

Peter Adeniyi Alaba, Ching Shya Lee, Faisal Abnisa, Mohamed Kheireddine Aroua, Yousif Abdalla Abakr, Mustapha Danladi Ibrahim, Patrick Cognet, Yolande Peres-Lucchese, Wan Mohd Wan Daud

► To cite this version:

Peter Adeniyi Alaba, Ching Shya Lee, Faisal Abnisa, Mohamed Kheireddine Aroua, Yousif Abdalla Abakr, et al.. Investigating the electrocatalytic oxidation of glycerol on simultaneous nitrogen- and fluorine-doped on activated carbon black composite. *Diamond and Related Materials*, 2020, 101, pp.107626. 10.1016/j.diamond.2019.107626 . hal-02648633

HAL Id: hal-02648633

<https://hal.science/hal-02648633>

Submitted on 29 May 2020

HAL is a multi-disciplinary open access archive for the deposit and dissemination of scientific research documents, whether they are published or not. The documents may come from teaching and research institutions in France or abroad, or from public or private research centers.

L'archive ouverte pluridisciplinaire **HAL**, est destinée au dépôt et à la diffusion de documents scientifiques de niveau recherche, publiés ou non, émanant des établissements d'enseignement et de recherche français ou étrangers, des laboratoires publics ou privés.



Open Archive Toulouse Archive Ouverte

OATAO is an open access repository that collects the work of Toulouse researchers and makes it freely available over the web where possible

This is an author's version published in: <http://oatao.univ-toulouse.fr/25850>

Official URL:

<https://doi.org/10.1016/j.diamond.2019.107626>

To cite this version:

Alaba, Peter Adeniyi and Lee, Ching Shya  and Abnisa, Faisal and Aroua, Mohamed Kheireddine and Abakr, Yousif Abdalla and Ibrahim, Mustapha Danladi and Cognet, Patrick  and Peres-Lucchese, Yolande  and Daud, Wan Mohd Wan *Investigating the electrocatalytic oxidation of glycerol on simultaneous nitrogen- and fluorine-doped on activated carbon black composite*. (2020) *Diamond and Related Materials*, 101. 107626. ISSN 0925-9635 .

Any correspondence concerning this service should be sent to the repository administrator: tech-oatao@listes-diff.inp-toulouse.fr

Investigating the electrocatalytic oxidation of glycerol on simultaneous nitrogen- and fluorine-doped on activated carbon black composite

Peter Adeniyi Alaba^a, Ching Shya Lee^{a,b,c,*}, Faisal Abnisa^d, Mohamed Kheireddine Aroua^{e,f}, Yousif Abdalla Abakr^g, Mustapha Danladi Ibrahim^{g,h}, Patrick Cognetⁱ, Yolande Pérèsⁱ, Wan Mohd Wan Daud^{a,**}

^a Department of Chemical Engineering, Faculty of Engineering, University of Malaya, 50603 Kuala Lumpur, Malaysia

^b University of Malaya, 50603 Kuala Lumpur, Malaysia

^c UMR5503 Laboratoire de Génie Chimique (LGC), France

^d Department of Chemical Engineering, Faculty of Engineering, King Abdulaziz University, Rabigh 21911, Saudi Arabia

^e Research Centre for nanomaterials and Energy Technology (RCNMET), School of Science and Technology, Sunway University, Bandar Sunway 47500, Malaysia

^f Department of Engineering, Lancaster University, Lancaster LA1 4YW, UK

^g Energy, Fuel and Power Technology Research Division, School of Engineering, the University of Nottingham Malaysia Campus, Jalan Broga, 43500 Semenyih, Selangor Darul Ehsan, Malaysia

^h Department of Chemical Engineering, Abubakar Tafawa Balewa University, P.M.B 0248, Bauchi, Nigeria

ⁱ Laboratory of Chemical Engineering (Labège), BP 84234 Campus INP-ENSIACET, 4 allée Emile Monso, 31432 Toulouse Cedex 4, France

A B S T R A C T

Keywords:

Activated carbon
Carbon black
Heteroatom doping
Nitrogen doping
Glycerol oxidation

To develop non-metallic electrocatalyst for glycerol electrooxidation, simultaneous co-doping of nitrogen and fluorine into activated carbon black (ACB) composite was explored to investigate the physical and electrochemical characteristics. The ACB was prepared by mixing activated carbon and carbon black. The N and F were incorporated using aniline and polytetrafluoroethylene as the precursors. The morphologies of the prepared samples were analyzed and the electrochemical behavior, as well as the electrocatalytic performance, was investigated in acid and alkaline environment. Porosity analysis shows that 20% N and F co-doped ACB (ACB-N₂F₂) reduced the surface area (491.64 m² g⁻¹) and increased the electroactive surface area, which could contribute to faster mass transport and electron transfer process to enhance the catalytic activity the electrode. The doping defect also reduced the charge transfer resistance, which could increase the spin densities and maximize charge re-distribution to generate more electroactive surface. The electrodes N-doped ACB (ACB-N₂) and ACB-N₂F₂ exhibited a remarkable electrocatalytic activity in alkaline medium, while only 30% N and F co-doped ACB electrode are suitable in acidic medium. Moreover, the catalyst displayed remarkable long-term stability/durability in alkaline environment.

1. Introduction

With the progress in advanced materials technology, development of electrocatalysts for alcohol electrooxidation is one of the big issues towards electrochemical energy conversion, value-added chemical production, and storage devices, like metal-air batteries, anion exchange membrane fuel cell (AEMFC) and polymer electrolyte fuel cells (PEFCs) [1–3]. Thus far, Pt-based materials are the most popularly utilized electrocatalyst for alcohol oxidation with high exchange current density [4]. Nevertheless, large scale application of Pt-based catalysts for production of value-added chemicals, AEMFCs and PEFCs is

prevented by scarcity, high cost, poisoning by carbonaceous reaction intermediate species and CO contaminants of the H₂ fuel are the major limitations of Pt catalysts [5]. Consequently, rational design of cost-effective Pt-free catalysts with high alcohol electrooxidation activity constitutes a great challenge. Therefore, several efforts have been channeled towards replacing Pt-based electrocatalysts in alcohol electrooxidations and fuel cell sciences [6,7]. Cheap earth-abundant metals like transition metal oxides, perovskites, and spinel based materials have been fabricated with the aim of achieving extremely active and durable non-precious metal as alternative electrocatalysts [8–10]. For instance, several authors have studied the transition metal oxides

* Correspondence to: C.S. Lee, University of Malaya, 50603 Kuala Lumpur, Malaysia.

** Corresponding author.

E-mail addresses: leecs@um.edu.my (C.S. Lee), ashri@um.edu.my (W.M.W. Daud).

supported by carbon materials like graphene, Activated carbon and Multiwalled carbon nanotubes (MWCNTs) [11–15]. Their reports show that carbon materials are viable support for non-precious metal catalysts since they possess high chemical and mechanical stability, inherent elasticity, corrosion resistance, surface area and outstanding conductivity. Although Hummers' methods or/and chemical vapor deposition (CVD) are generally implemented for the synthesis of graphene oxide/graphene sheets. The feasibility of graphene-based materials for various industrial applications is limited because of high cost and environmental concerns since hazardous reagents are used. On the other hand, MWCNT is easy to prepare, and their geometrical and morphological features are tunable via well-established and adaptable preparation procedures. Moreover, Weber et al. [16] utilized activated carbon as a support for Pd using Atomic Layer Deposition and reported a remarkable performance towards glycerol electrooxidation.

Lately, carbon matrix functionalized with heteroatoms like fluorine (F) phosphorous (P), sulfur (S), boron (B) and nitrogen (N) individually or in combination has been examined as a promising electrocatalyst capable of replacing the Pt-based [17]. Prominent of all the heteroatom doped carbon electrocatalysts is N doped carbon, which displays better activity. For instance, several authors have reported that the catalytic activity of N doped carbon during ORR is on par with conventional Pt/C in alkaline medium [18–20]. However, N doped carbon exhibits much lower catalytic performance in comparison with Pt/C in acidic solutions. Furthermore, simultaneous co-doped N and F into carbon matrix are proposed to induce maximum charge delocalization on the adjacent carbon atoms. This significantly improves adsorption of oxygen and its subsequent reduction than the single N doped carbon [21,22]. The simultaneous doping of N and F greatly increased the bond distance of O₂ due to its superior electron density and more polarization in the C–N, C–F, and C–C bonds helped to increase the kinetics of ORR. Moreover, Wood et al. [23] and Peera et al. [24] reported that F doping also enhanced the long-time stability of N-doped carbons in acidic solutions. Recently, Peera et al. [24] reported the synthesis graphite nanofibers (N-F/GNFs) simultaneously co-doped N and F. The synergistic effect of N and F on the morphology of N-F/GNFs and catalytic activity in acidic media during ORR were studied. They observed that the interlayer spacing between the GNF layers increases with increasing electronegativity of F when combined with N. Moreover, structural transformation occurred to the crumpled graphene sheets with several open-edge active sites, which facilitates a remarkable catalytic activity during ORR. This level of catalytic activity is not achievable with single doping on GNF matrix using N [24].

With this impetus, this study explored, simultaneous co-doping of N and F into activated carbon composite by a simple blending, and heat treatment method and investigated the morphological evolution. The electrocatalytic activity during glycerol oxidation was studied. The effect of N and F co-doping on the maximum charge delocalization on the carbon matrix due to electronegativity difference between N and F and the interlayer spacing between the sample layers were studied.

2. Materials and methods

2.1. Materials

Activated carbon (99.5% purity, CAS: 7440-44-0, average particle size 100 nm and 950 m² g⁻¹ specific surface area), Paraffin oil (98%, CAS: 8012-95-1), aniline (99%, CAS: 62-53-3), KOH (86%, CAS: 1310-58-3) and polytetrafluoroethylene (PTFE 60% dispersion in H₂O, CAS:9002-84-0) were procured from Sigma-Aldrich. Carbon black Super P (99% purity, Cat.Nr. PL-CB13-100 g, specific surface area of 550 m² g⁻¹ and average particle size of 13 nm) was purchased from PlasmaChem.

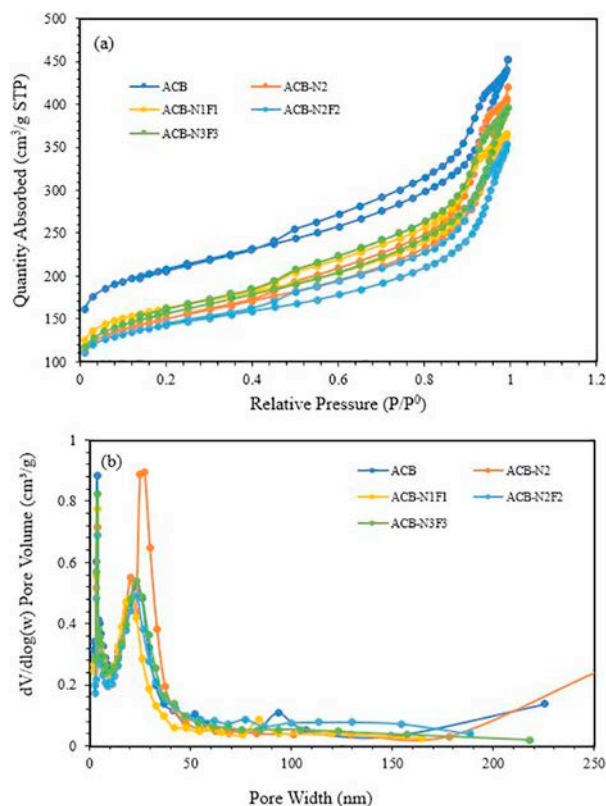


Fig. 1. N₂ adsorption/desorption isotherms (a) and the corresponding pore size distributions (b) of ACB and heteroatom doped ACB.

Table 1

The textural parameters of ACB and heteroatom doped ACB.

Samples	SBET (m ² g ⁻¹)	Ex-SBET (m ² g ⁻¹)	PSD (nm)	V _{micro} (cm ³ g ⁻¹)	V _{total} (cm ³ g ⁻¹)
ACB	715	314	6.50	0.1843	0.6691
ACB-N ₂ F ₂	491	228	8.25	0.1208	0.5334
ACB-N ₁ F ₁	559	259	7.19	0.1372	0.5550
ACB-N ₃ F ₃	543	295	7.29	0.1133	0.6015
ACB-N ₂	519	296	8.40	0.1115	0.6196

2.2. Synthesis of activated carbon black (ACB) composite

The ACB material was synthesized by blending 20 wt% CB Nano powder and 80 wt% activate carbon powder.

2.3. Synthesis of heteroatom doped ACB nanocomposites

ACB-NF was synthesized by adding 10 g of the prepared ACB to a solution containing 10 g of 1,3 propanediol, 2 g PTFE, 2 g aniline and 100 mL water. The mixture was stirred to evaporate the solvent in a fume cupboard at ambient temperature. The resulting mixture was dried at 100 °C overnight and calcined for 1 h at 1000 °C in high pure N₂, with a heating rate of 20 °C min⁻¹. The resulting samples are designated as ACB-N₂F₂. The content of the PTFE and aniline were varied in the precursor (1, 2 and 3 g). The resulting samples are designated ACB-N_mF_m, where m represents the mass of the PTFE and aniline in the precursor.

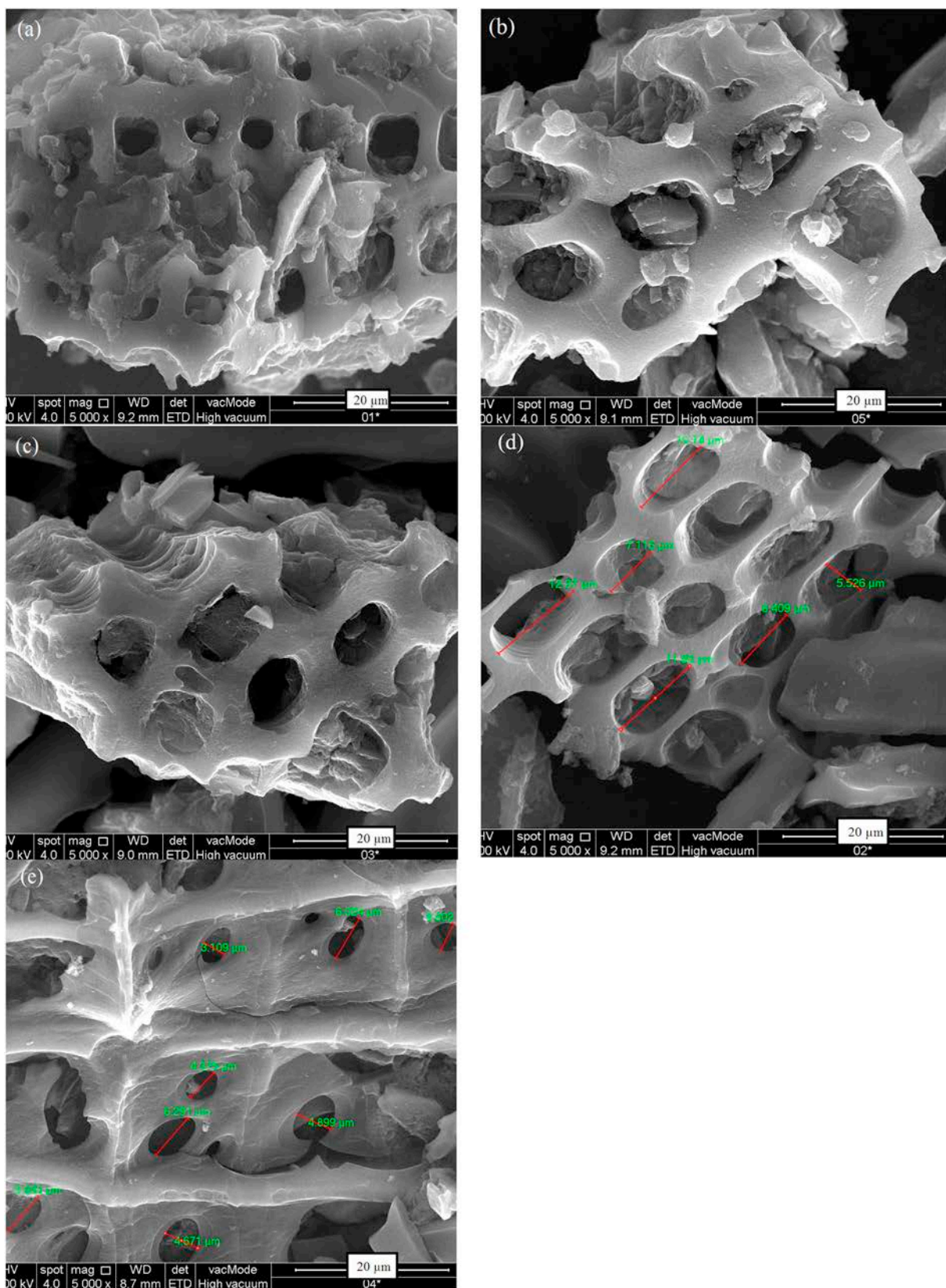


Fig. 2. FESEM images of (a) ACB; (b) ACB-N₂; (c) ACB-N₁F₁; (d) ACB-N₂F₂; (e) ACB-N₃F₃.

2.4. Physicochemical characterizations

X-ray diffractometer (Seifert X-ray Diffractometer JSO 2002) was used to record the XRD pattern for all the prepared heteroatom doped

carbon composite using nickel filtered Cu K α radiation ($\lambda = 1.544 \text{ \AA}$) ranging from 5.018 to 69.966° (2 θ) and 0.026° as the step size. The Nitrogen adsorption/desorption analysis was performed with the aid of surface area and porosity analyzer (Micrometrics ASAP 2020) under

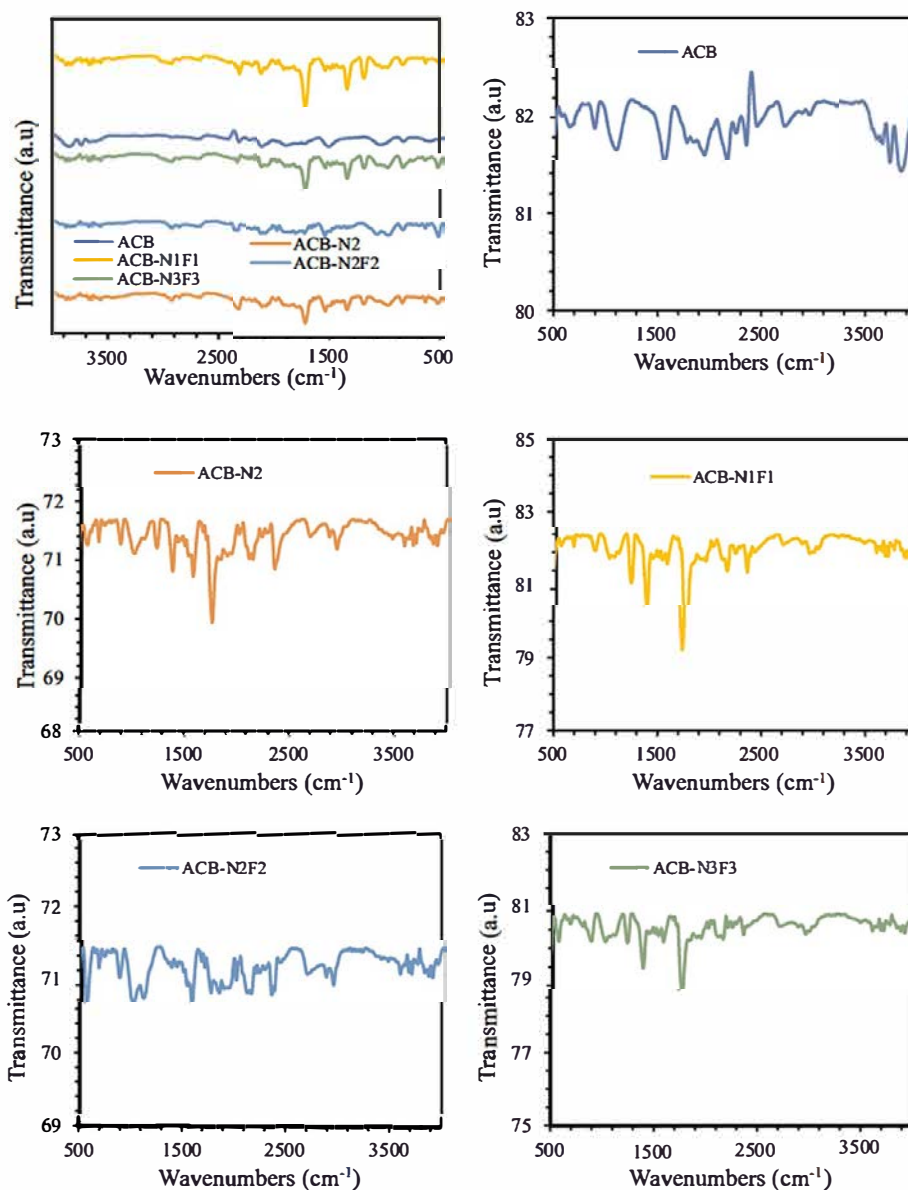


Fig. 3. FT-IR spectra of ACB and heteroatom doped ACB.

analysis bath Temperature of 77.350 K as described by [25,26]. Perkin Elmer Spectrum RX FT-IR was employed for the infrared spectroscopy (IR) to check the existing functional groups in the prepared heteroatom doped carbon composite of 77.350 K described by [27]. Field Emission Scanning electron microscope/Energy Dispersive X-ray (FESEM/EDX), FEI Quanta 400 FE-SEM as the accelerating voltage to check the morphology of the prepared heteroatom doped carbon composite is 20 kV. Prior to the scanning, the samples were coated with gold to enhance the electrical conductivity as described by Alaba et al. [28].

2.5. Electrochemical measurements

To evaluate the catalytic activities of these electrocatalysts, cyclic voltammograms analysis was conducted in an electrolyte comprising 1.0 M KOH and 1.0 M glycerol at a potential range of -0.5 to 1 V (vs SHE) using 50 mV s^{-1} as the sweeping rate. Prior to the electrochemical measurements, the catalyst pastes were prepared by blending the composite samples with paraffin oil (70:30, w%) in a mortar and pestle for 30 min. About 25 mg of the paste was compactly filled into a PTFE Teflon rod (4.5 mm internal diameter with 2 mm depth). A 3 mm

stainless rod was connected to the paste through the other end of the rod. All the electrochemical tests were performed using BioLogic Science instrument with EC-Lab Software. The electroactive surface area (ECSA) of anodes was determined using the Randles-Sevcik formula [28]

$$I_p = 2.69 \times 10^5 \times AD^{1/2}n^{3/2}\gamma^{1/2}C$$

where n is the number of the electrons taking part in the oxidation reaction, A is the electrode surface area of the (cm^2), γ is the scan rate of the potential perturbation (V s^{-1}), D is the diffusion coefficient of the molecules in the electrolyte (cm^2s^{-1}), and C is the concentration of the probe molecule in the bulk solution (mol cm^{-3}).

3. Results and discussion

3.1. Characterization of NF-ACC nanocomposites

Fig. 1 presents the N_2 adsorption/desorption isotherms and the corresponding pore size distributions of ACB and heteroatom doped ACB. All the samples exhibit a typical type IV isotherm with an obvious

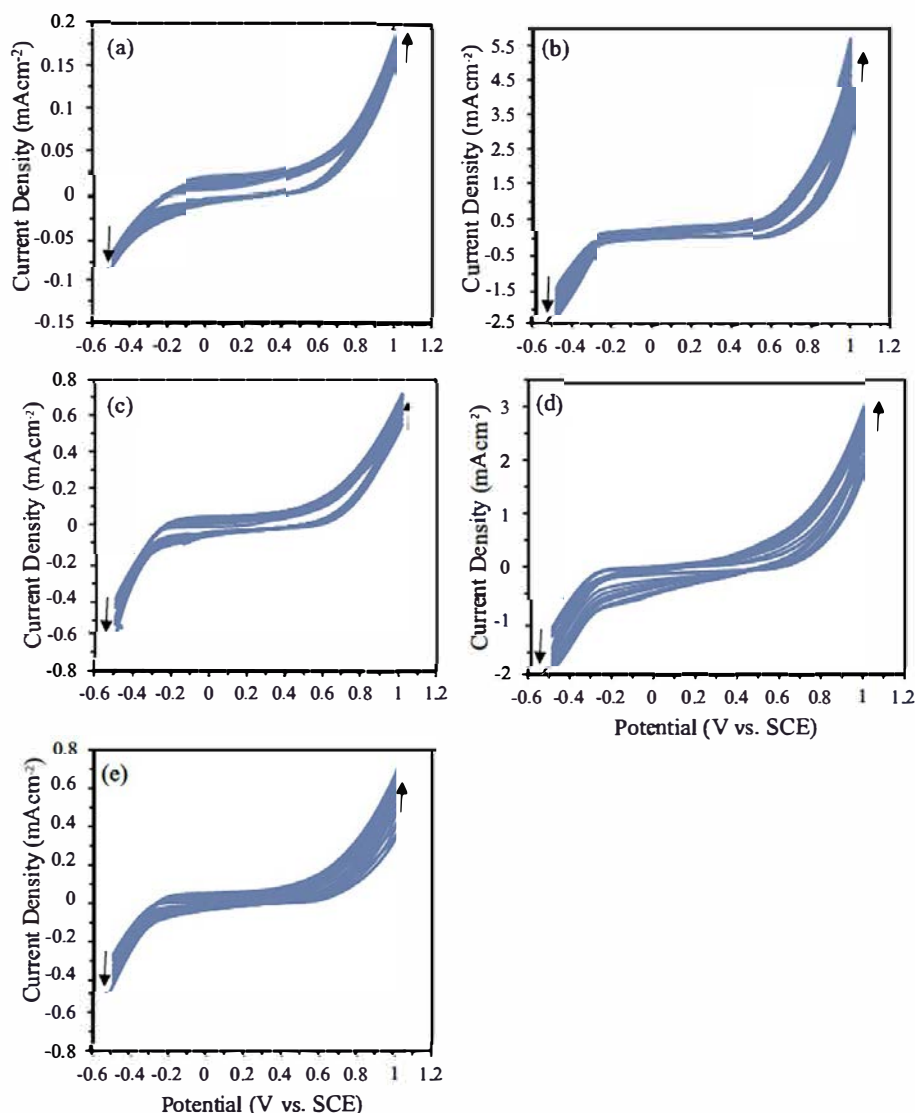


Fig. 4. A series of CVs during 10 consecutive potential cycles of (a) ACB; (b) ACB-N₂; (c) ACB-N₁F₁; (d) ACB-N₂F₂; (e) ACB-N₃F₃ electrode in a 1.0 M KOH solution between -0.5 and 1.0 V at $v = 50 \text{ mV s}^{-1}$.

H4 type hysteresis loop (with numerous slit-shaped pores) ascribed to capillary condensation in the mesopores at high pressures of $P/P^0 > 0.8$, which indicates synchronicity of mesopores and micropores in ACB and heteroatom doped ACB [29]. Table 1 reveals the details of the porosity parameter of all the composite samples. This shows that the heteroatom doping leads to a reduction in the Brunauer-Emmett-Teller (BET) specific surface area (V) with a corresponding increase in pore size. The sample ACB-N₂F₂ followed by ACB-N₂ has the lowest SBET (491 and 519 $\text{m}^2 \text{g}^{-1}$) and the highest pore size, which could contribute to faster mass transport and electron transfer process, which could enhance the catalytic activity the charge [30].

Fig. 2 presents the FESEM image of the composite ACB and the heteroatom doped ACB samples. The image of all the samples at $20 \mu\text{m}$ shows a typical image of metal-free amorphous carbon structure. The EDX results in Fig. S1 also confirm that the metal-free amorphous carbon structure, showing that the heteroatoms are homogeneously doped in the carbon matrix and the heteroatoms were removed during calcination but caused a structural effect capable of influencing the electrocatalytic performance of the carbon composites. The FESEM images also confirm the doping effect revealed by the nitrogen adsorption/desorption analysis results. The reduction in the SBET is due to the collapse of some of the pore walls as the pore width increase. The

level of pore wall collapse corresponds with the level of doping.

Fig. S2(a) presents large-angle XRD patterns of the ACB and heteroatom doped ACB electrocatalysts, which reveals two broad amorphous peaks that appear at approximately 24.59° and 43.31° for all the samples, regardless of the level of doping. The two peaks correspond to the C(0 0 2) and C(1 0 1) diffraction planes [29,31]. Moreover, no sample reveals another distinguishable peak, signifying that the samples are mostly amorphous carbon, being consistent with the results of FESEM and EDX [29].

Fig. 3 presents the FT-IR spectra of ACB and heteroatom doped ACB. The spectrum in deep blue line shows the functional groups characterized with ACB, which includes the stretching vibrations at $1085, 1750, 2848-2933,$ and $3618-3858 \text{ cm}^{-1}$, corresponding to $-\text{C}-\text{O}, -\text{C}=\text{O}, \text{C}-\text{H},$ and $\text{O}-\text{H}$ group. The doping effect of F is confirmed by the emergence of the bands at $1077, 1098-1101, 1217-1236 \text{ cm}^{-1}$, which are stretching vibrations of $\text{C}-\text{F}$ (semi-ionic $\text{C}-\text{F}$ bond and ionic $\text{C}-\text{F}$ bond) [32]. The presence of N is confirmed by the presence of the bands around $1368-1370, 1421-1488, 1516-1521 \text{ cm}^{-1}$, which are stretching vibrations of $-\text{C}-\text{N}-$ group [29,33]. Moreover, doping with heteroatoms leads to reduction in the absorbance baseline. The reduction caused by N doping is more severe than that of F doping. The shifts in the $\text{O}-\text{H}$ vibration are indicative of

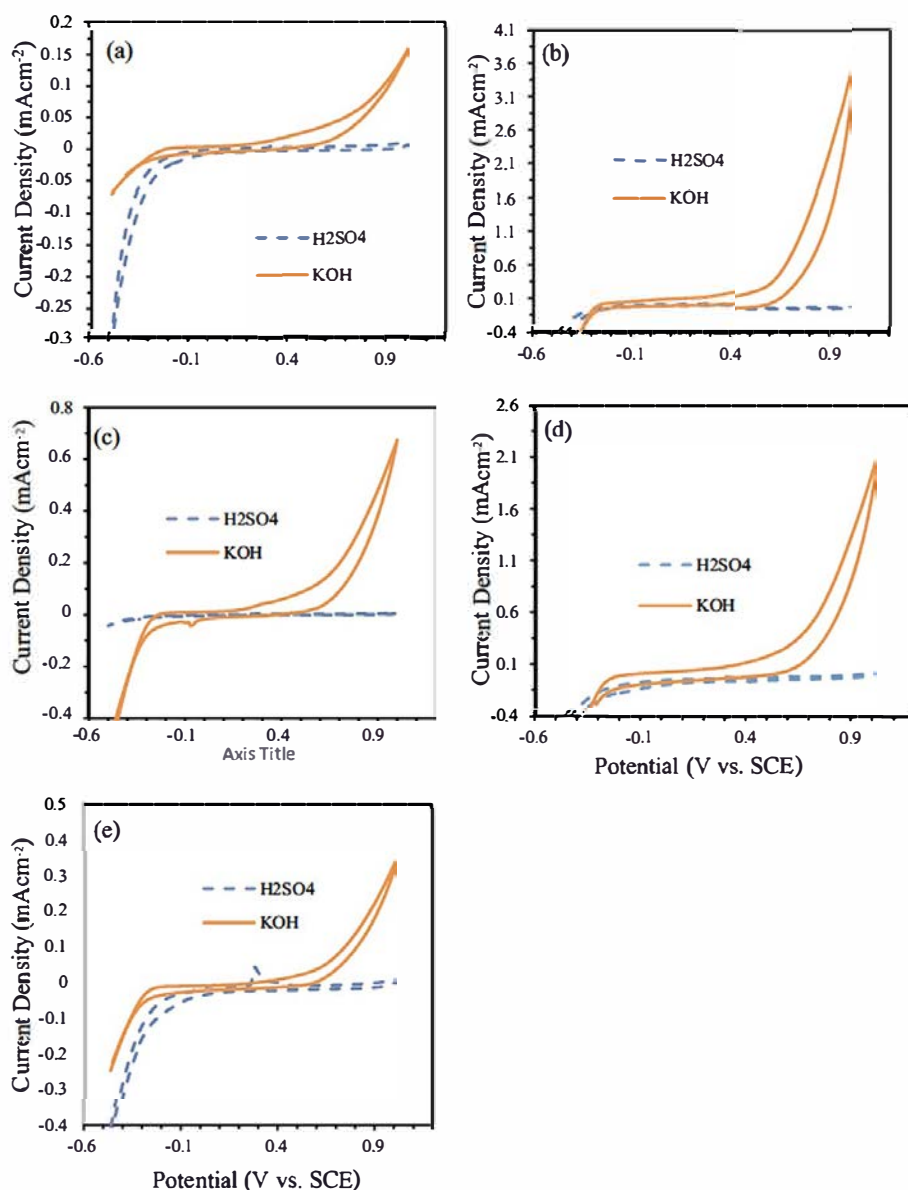


Fig. 5. Electrochemical responses of (a) ACB; (b) ACB-N₂; (c) ACB-N₁F₁; (d) ACB-N₂F₂; (e) ACB-N₃F₃; in 1.0 M KOH and 1.0 M H₂SO₄.

heteroatom doping, including introduction of $-NH-$ and $-N-$ functional groups. The intensity was greatly enhanced in ACB-N₃F₃ [33].

3.2. Electrochemical characterization

The value ECSA was determined using the Randles-Sevcik formula and 12.42, 122.53, 13.72, 146.64, and 31.95 $\text{cm}^2 \text{g}^{-1}$ were obtained for ACB, ACB-N₂, ACB-N₁F₁, ACB-N₂F₂, and ACB-N₃F₃. These results reveal that rational heteroatom doping can significantly boost the ECSA value of ACB composite electrocatalyst. The best ECSA is exhibited by ACB-N₂F₂, which is over 10 times higher than that of ACB.

The novel electrodes were characterized using consecutive CV between -0.5 and 1.0 V at 50 mV s^{-1} for 10 cycles was performed in 1 M KOH solution (Fig. 4). Fig. 4 reveals the peak current density of the forward scan increases with an increasing number of cycles, while that of the backward scan shifts towards the negative current. Doping of the heteroatoms improves the oxygen evolution potential of the activated carbon composite material. Of all the doped carbon materials, ACB-N₂ shows the highest activity followed by ACB-N₂F₂ and ACB-N₃F₃, while ACB-N₁F₁ has the lowest activity in a solution containing 1 M of KOH.

A different set of electrodes was used in a solution containing 1 M of H₂SO₄. The pH of the electrolyte solution largely influences the redox behavior of the film [34,35]. Fig. 5 reveals a comparative illustration of the redox activity in both acidic and alkaline supporting electrolytes. The alkaline environment is a more promising redox electrode. This is contrary to other reports of carbon paste electrodes [35]. While the electrodes prove to be bifunctional in alkaline solution, it is only promising for oxygen reduction reaction (ORR) in acidic medium, except for ACB-N₃F₃, which shows a well-defined oxidation peak.

3.3. Electrooxidation of glycerol

Electrooxidation of glycerol was studied in a CV experiment between -0.5 and 1.0 V at 50 mV s^{-1} using 1 M KOH as the supporting electrolyte. Fig. 6 presents the CV results of the electrode performance with and without 1 M glycerol. The addition of 1 M glycerol to the alkaline solution significantly boosts the electrochemical response of ACB-N₂ and ACB-N₂F₂ electrodes. It is noteworthy that based on a specific activity (mA/cm^2), ACB-N₂ exhibits the highest glycerol oxidation activity (Fig. 6b), while based on mass activity (mA/mg), ACB-

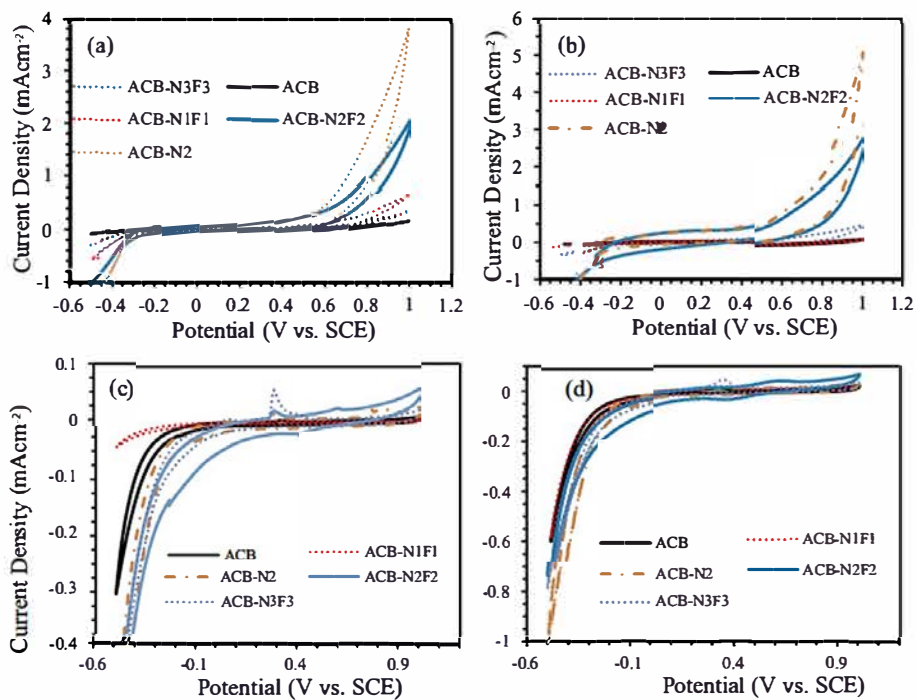


Fig. 6. Electrochemical response of the electrodes in (a) 1 M KOH; (b) 1 M glycerol + 1 M KOH; (c) 1 M H₂SO₄; (d) 1 M glycerol + 1 M H₂SO₄.

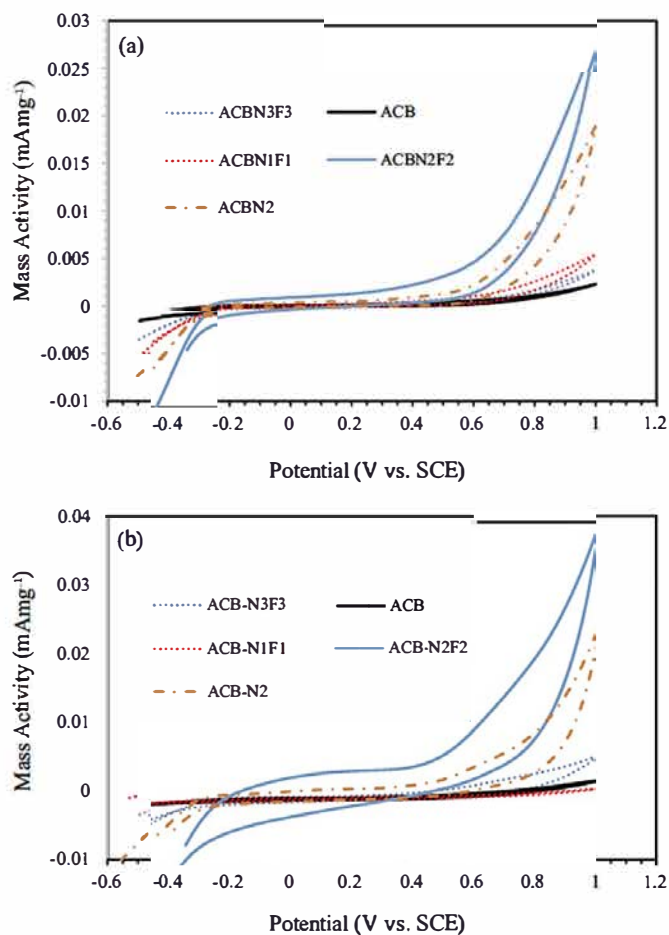


Fig. 7. Mass activity of the electrodes in (a) 1 M KOH; (b) 1 M glycerol + 1 M KOH.

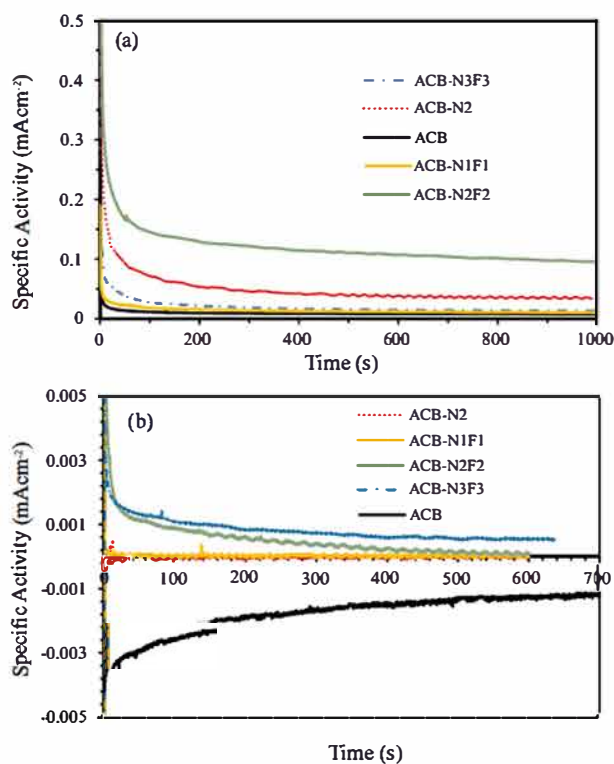


Fig. 8. Chronoamperometric measurements of the electrodes at 0.5 V in (a) 1 M glycerol + 1 M KOH; (b) 1 M glycerol + 1 M H₂SO₄.

N₂F₂ exhibits the best activity (Fig. 7). The remarkable mass activity of ACB-N₂F₂ is because nitrogen and fluorine have higher electronegativity difference, which can synergistically tune the electronic structure to favor oxygen evolution reaction. The synergistic effect of nitrogen and fluorine doping on the composite carbon material induces defects, which could provoke high spin densities and maximum charge re-distribution to produce many electroactive sites that synergistically

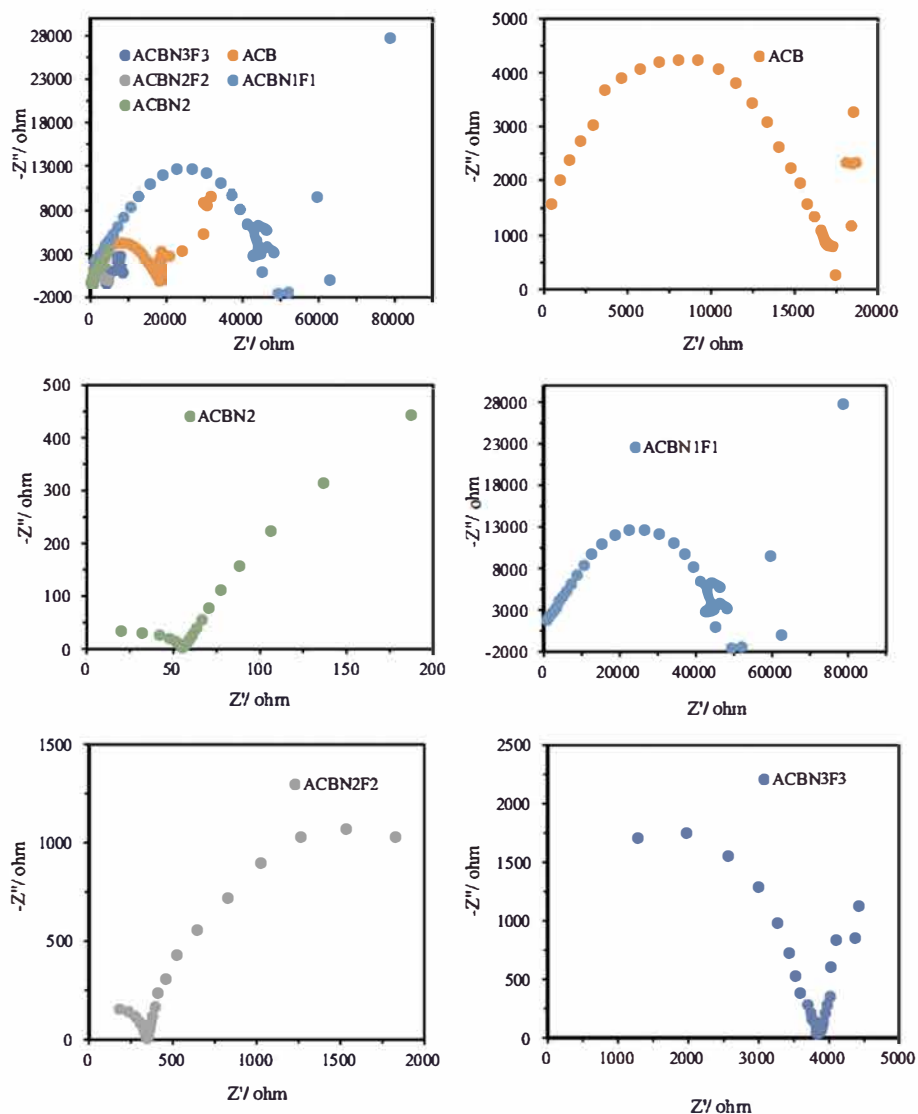


Fig. 9. Nyquist plots of the carbon composite electrocatalysts operated in 1 M glycerol + 1 M KOH solution at the potential of -0.1 V.

promote glycerol oxidation [36–38].

The linear sweep voltammetry results also confirm the observation regarding the specific activity and mass activity of ACB-N₂ and ACB-N₂F₂ electrodes (Fig. S3). The glycerol oxidation activity of the electrodes was also tested in the presence of 1 M H₂SO₄. The performance of the electrodes in 1 M H₂SO₄ and 1 M glycerol + 1 M H₂SO₄ were presented in Fig. 6 (c) and (d). Of all the electrodes, only ACB-N₃F₃ exhibits a little significant electrocatalytic activity towards glycerol oxidation.

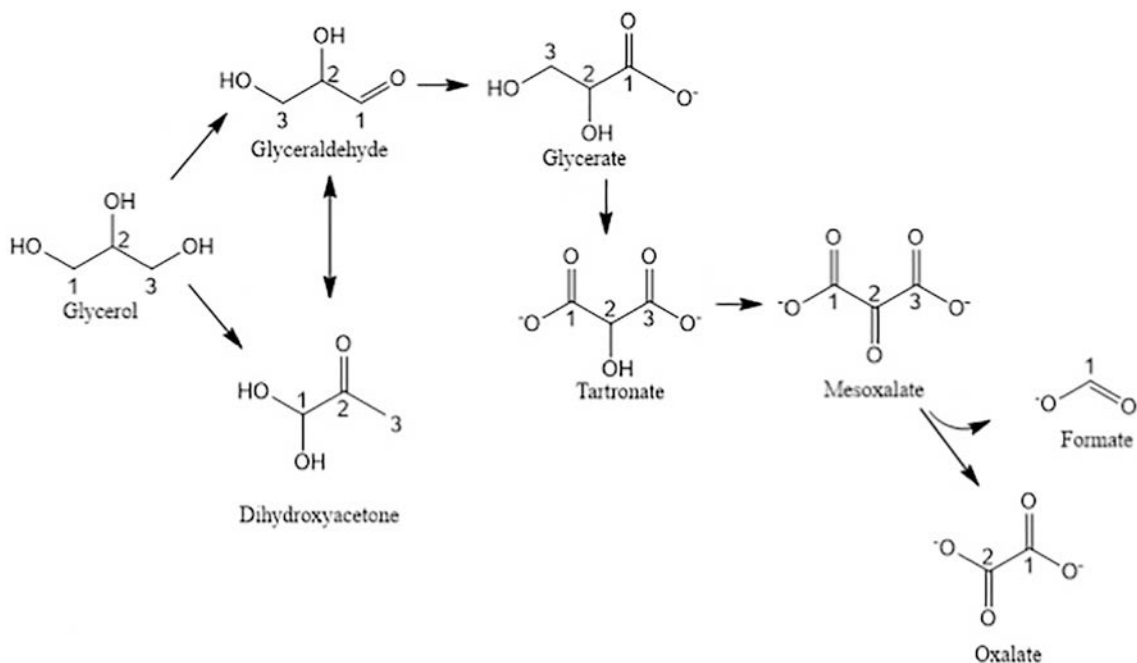
3.4. Electrocatalytic performance using chronoamperometry

Fig. 8 presents the chronoamperometric measurements of the electrodes in 1 M glycerol + 1 M KOH and 1 M glycerol + 1 M H₂SO₄. This measurement reveals the electrochemical activity and stability of the electrodes. Initially, the conversion of glycerol occurred rapidly in both acidic and alkaline environment and then reach a constant state for all the electrodes. A higher current density at the end of the experiment indicates better catalytic performance. The activity order is ACB < ACB-N₁F₁ < ACB-N₃F₃ < ACB-N₂ < ACB-N₂F₂ in the alkaline environment, while the activity order is ACB-N₃F₃ > ACB-N₂F₂ in acidic environment. These results show that ACB-N₂F₂ is the best electrocatalyst and alkaline media is the most suitable for glycerol oxidation, using heteroatom-doped activated carbon black composite. It is also

worthy to note that ACB is only suitable for glycerol reduction (ORR).

3.5. Electrochemical impedance spectroscopy (EIS)

Fig. 9 presents the electrochemical impedance spectroscopy (EIS) at the potential of -0.1 V, which unravels the resistance to the electrochemical reaction processes of the electrocatalysts. The results show that doping with heteroatom helps to decrease the x-intercept of ACB composite, thereby minimizing the bulk resistance (R_s), which is the resistance of electrolyte solution, inherent resistance of the active surface of the electrode, and the contact resistance at the interface between the current collector electrocatalyst [39]. The double-layer capacitance (C_{dl}) in parallel with the charge transfer resistance (R_{ct}) at the interface of the electrode/electrolyte is reflected by the small semicircle (quasi-semicircle or Diameter impedance arc (DIA)) in the plots [40,41]. The quasi-semicircle is an important parameter for determining the electrical conductivity of the fabricated activated carbon black composite electrocatalysts. The order of diameter of the quasi-semicircle of these composite electrocatalysts is as follows: ACBN₁F₁ > ACB > ACBN₂F₂ > ACBN₂F₂ > ACBN₂. This result shows that ACBN₂ followed by ACBN₂F₂ exhibits the smallest electron transfer resistance and the best electrical conductivity. However, ACBN₂F₂ exhibits a better electrocatalytic performance than ACBN₂, showing that nitrogen doping is responsible for the declined electron transfer resistance,



Scheme 1. Reaction mechanism proposed for the electrooxidation of glycerol on ACBN₂F₂.

while the synergistic effect of nitrogen and fluorine glycerol oxidation activity.

Furthermore, ACBN₂ and ACBN₂F₂ showed an immense performance improvement towards glycerol electrooxidation when compared with ACB. The improved activity could be ascribed to the defect created on the carbon structure by the optimal heteroatom doping, which improved the hydrophilicity of its surface with an increase in the hydrophilic functional groups, thereby promoting the mass transfer between the electrolyte and the heteroatom doped ACB composites [42]. Furthermore, heteroatom doping supplies additional electron to the ACB substrates readily, meaning that the resistance to the flow of electron is minimized [43]. The expected products of glycerol electrooxidation using ACBN₂F₂ include valuable compounds like glycerate, dihydroxyacetone, tartronate, mesoxalate, etc. (Scheme 1), which could effectively minimize the costs of production of H₂ [16].

4. Conclusion

Nitrogen- and fluorine-doped ACB composite were successfully synthesized using aniline and PTFE as precursors in the presence of 1,3 propanediol and distilled water. Previously, heteroatom doped carbon materials have been successfully used for oxygen reduction reaction. We have revealed that rationally designed nitrogen and fluorine simultaneously doped ACB composite is suitable for glycerol oxidation. The results of the XRD, FTIR BET, and FESEM of the doped samples show that the doping was successful, and the doping effect reflects in the electrochemical behavior. The sample ACB-N₂F₂ has the lowest SBET (491 m² g⁻¹) and the highest electroactive surface area (146.64 cm² g⁻¹), which could contribute to faster mass transport and electron transfer process to enhance the catalytic activity. The doping defect also reduced the charge transfer resistance, which could increase the spin densities and maximize charge re-distribution to produce the highest number electroactive sites.

ACB-N₂ and ACB-N₂F₂ electrodes exhibit a remarkable activity in alkaline medium, while only the ACB-N₃F₃ electrode is suitable in acidic medium. The superior mass activity of ACB-N₂F₂ is due to high electronegativity difference of nitrogen and fluorine, which can synergistically tune the electronic structure to favor glycerol oxidation reaction. The activity order is ACB < ACB-N₁F₁ < ACB-N₃F₃ < ACB-

N₂ < ACB-N₂F₂ in the alkaline environment, while the activity order is ACB-N₃F₃ > ACB-N₂F₂ in acidic environment. These results show that ACB-N₂F₂ is the best electrocatalyst and alkaline media is the most suitable for glycerol oxidation, using heteroatom-doped carbon composite.

Declaration of competing interest

The authors declare that they have no known competing financial interests or personal relationships that could have appeared to influence the work reported in this paper.

Acknowledgments

The authors acknowledge the Fundamental Research Grant Scheme (FRGS) from the Ministry of Education, Malaysia (Department of Higher Education), for funding this work through Project No. "FP046-2017A".

Appendix A. Supplementary data

Supplementary data to this article can be found online at <https://doi.org/10.1016/j.diamond.2019.107626>.

References

- [1] F. Cheng, J. Chen, Metal-air batteries: from oxygen reduction electrochemistry to cathode catalysts, *Chem. Soc. Rev.* 41 (2012) 2172–2192.
- [2] Y. Liang, Y. Li, H. Wang, H. Dai, Strongly coupled inorganic/nanocarbon hybrid materials for advanced electrocatalysis, *J. Am. Chem. Soc.* 135 (2013) 2013–2036.
- [3] F.H. Liu, C.X. Lin, E.N. Hu, Q. Yang, Q.G. Zhang, A.M. Zhu, Q.L. Liu, Anion exchange membranes with well-developed conductive channels: effect of the functional groups, *J. Membr. Sci.* 564 (2018) 298–307.
- [4] H.A. Gasteiger, S.S. Kocha, B. Sompalli, F.T. Wagner, Activity benchmarks and requirements for Pt, Pt-alloy, and non-Pt oxygen reduction catalysts for PEMFCs, *Appl. Catal. B Environ.* 56 (2005) 9–35.
- [5] Z.-Y. Wu, P. Chen, Q.-S. Wu, L.-F. Yang, Z. Pan, Q. Wang, Co/Co₃O₄/C-N, a novel nanostructure and excellent catalytic system for the oxygen reduction reaction, *Nano Energy* 8 (2014) 118–125.
- [6] Y. Liang, H. Wang, P. Diao, W. Chang, G. Hong, Y. Li, M. Gong, L. Xie, J. Zhou, J. Wang, Oxygen reduction electrocatalyst based on strongly coupled cobalt oxide nanocrystals and carbon nanotubes, *J. Am. Chem. Soc.* 134 (2012) 15849–15857.
- [7] J. Zhang, T. Zhu, Y. Liang, C. Zhang, S. Shi, C. Xu, CeO₂ promoted Au/C catalyst for

- glycerol electro-oxidation in alkaline medium, *J. Energy Inst.* 89 (2016) 325–329.
- [8] F. Cheng, T. Zhang, Y. Zhang, J. Du, X. Han, J. Chen, Enhancing electrocatalytic oxygen reduction on MnO₂ with vacancies, *Angew. Chem.* 125 (2013) 2534–2537.
- [9] Q. Tang, L. Jiang, J. Liu, S. Wang, G. Sun, Effect of surface manganese valence of manganese oxides on the activity of the oxygen reduction reaction in alkaline media, *ACS Catal.* 4 (2014) 457–463.
- [10] E. Fabbri, R. Mohamed, P. Levecque, O. Conrad, R. Kötzt, T.J. Schmidt, Composite electrode boosts the activity of Ba_{0.5}Sr_{0.5}Co_{0.8}Fe_{0.2}O_{3-δ} perovskite and carbon toward oxygen reduction in alkaline media, *ACS Catal.* 4 (2014) 1061–1070.
- [11] L. Yang, S. Jiang, Y. Zhao, L. Zhu, S. Chen, X. Wang, Q. Wu, J. Ma, Y. Ma, Z. Hu, Boron-doped carbon nanotubes as metal-free electrocatalysts for the oxygen reduction reaction, *Angew. Chem. Int. Ed.* 50 (2011) 7132–7135.
- [12] C. Gupta, P.H. Maheshwari, D. Sachdev, A. Sahu, S. Dhakate, Highly purified CNTs: an exceedingly efficient catalyst support for PEM fuel cell, *RSC Adv.* 6 (2016) 32258–32271.
- [13] I. Kruusenberg, D. Ramani, S. Ratso, U. Joost, R. Saar, P. Rauwel, A.M. Kannan, K. Tammeveski, Cobalt–nitrogen Co-doped carbon nanotube cathode catalyst for alkaline membrane fuel cells, *ChemElectroChem* 3 (2016) 1455–1465.
- [14] S.P. Amyab, E. Saievar-Iranizad, A. Bayat, Platinum nanoparticles with superacid-doped polyvinylpyrrolidone coated carbon nanotubes: electrocatalyst for oxygen reduction reaction in high-temperature proton exchange membrane fuel cell, *RSC Adv.* 6 (2016) 41937–41946.
- [15] M. Beltrán-Gastélum, M. Salazar-Gastelum, R. Felix-Navarro, S. Pérez-Sicairos, E. Reynoso-Soto, S. Lin, J. Flores-Hernandez, T. Romero-Castanon, I. Albarran-Sanchez, F. Paraguay-Delgado, Evaluation of PtAu/MWCNT (multiwalled carbon nanotubes) electrocatalyst performance as cathode of a proton exchange membrane fuel cell, *Energy* 109 (2016) 446–455.
- [16] M. Weber, P. Collot, H. El Gaddari, S. Tingry, M. Bechelany, Y. Holade, Enhanced catalytic glycerol oxidation activity enabled by activated-carbon-supported palladium catalysts prepared through atomic layer deposition, *ChemElectroChem* 5 (2018) 743–747.
- [17] M. Weber, N. Tuleushova, J. Zgheib, C. Lamboux, I. Iatsunskiy, E. Coy, V. Flaud, S. Tingry, D. Cornu, P. Miele, Enhanced electrocatalytic performance triggered by atomically bridged boron nitride between palladium nanoparticles and carbon fibers in gas-diffusion electrodes, *Appl. Catal. B Environ.* 257 (2019) 117917.
- [18] Y. Li, W. Zhou, H. Wang, L. Xie, Y. Liang, F. Wei, J.-C. Idrobo, S.J. Pennycook, H. Dai, An oxygen reduction electrocatalyst based on carbon nanotube–graphene complexes, *Nat. Nanotechnol.* 7 (2012) 394.
- [19] P. Chen, T.Y. Xiao, Y.H. Qian, S.S. Li, S.H. Yu, A nitrogen-doped graphene/carbon nanotube nanocomposite with synergistically enhanced electrochemical activity, *Adv. Mater.* 25 (2013) 3192–3196.
- [20] S. Chen, J. Bi, Y. Zhao, L. Yang, C. Zhang, Y. Ma, Q. Wu, X. Wang, Z. Hu, Nitrogen-doped carbon nanocages as efficient metal-free electrocatalysts for oxygen reduction reaction, *Adv. Mater.* 24 (2012) 5593–5597.
- [21] X. Sun, Y. Zhang, P. Song, J. Pan, L. Zhuang, W. Xu, W. Xing, Fluorine-doped carbon blacks: highly efficient metal-free electrocatalysts for oxygen reduction reaction, *ACS Catal.* 3 (2013) 1726–1729.
- [22] X. Sun, P. Song, T. Chen, J. Liu, W. Xu, Fluorine-doped BP 2000: highly efficient metal-free electrocatalysts for acidic oxygen reduction reaction with superlow H₂O₂ yield, *Chem. Commun.* 49 (2013) 10296–10298.
- [23] K.N. Wood, S. Pylypenko, T.S. Olson, A.A. Dameron, K. O'Neill, S.T. Christensen, H.N. Dinh, T. Gennett, R. O'Hayre, Effect of halide-modified model carbon supports on catalyst stability, *ACS Appl. Mater. Interfaces* 4 (2012) 6728–6734.
- [24] S.G. Peera, A. Sahu, A. Arunchander, S. Bhat, J. Karthikeyan, P. Murugan, Nitrogen and fluorine co-doped graphite nanofibers as high durable oxygen reduction catalyst in acidic media for polymer electrolyte fuel cells, *Carbon* 93 (2015) 130–142.
- [25] P.A. Alaba, Y.M. Sani, W.M.A.W. Daud, Synthesis and characterization of hierarchical nanoporous HY zeolites from acid-activated kaolin, *Chin. J. Catal.* 36 (2015) 1846–1851.
- [26] P.A. Alaba, Y.M. Sani, I.Y. Mohammed, Y.A. Abakr, W.M.A.W. Daud, Synthesis and application of hierarchical mesoporous HZSM-5 for biodiesel production from shea butter, *J. Taiwan Inst. Chem. Eng.* 59 (2016) 405–412.
- [27] P.A. Alaba, Y.M. Sani, I.Y. Mohammed, Y.A. Abakr, W.M.A.W. Daud, Synthesis of hierarchical nanoporous HY zeolites from activated kaolin, a central composite design optimization study, *Adv. Powder Technol.* 28 (2017) 1399–1410.
- [28] P.A. Alaba, Y.M. Sani, I.Y. Mohammed, Y.A. Abakr, W.M.A.W. Daud, Synthesis and characterization of sulfated hierarchical nanoporous faujasite zeolite for efficient transesterification of shea butter, *J. Clean. Prod.* 142 (2017) 1987–1993.
- [29] H.-J. Zhang, S. Yao, J. Geng, Z.-F. Ma, J. Yang, Oxygen reduction reaction with efficient, metal-free nitrogen, fluoride-codoped carbon electrocatalysts derived from melamine hydrogen fluoride salt, *J. Colloid Interface Sci.* 535 (2019) 436–443.
- [30] S. Fu, C. Zhu, J. Song, M.H. Engelhard, B. Xiao, D. Du, Y. Lin, Nitrogen and fluorine-codoped carbon nanowire aerogels as metal-free electrocatalysts for oxygen reduction reaction, *Chem Eur J* 23 (2017) 10460–10464.
- [31] J. Duan, S. Chen, M. Jaroniec, S.Z. Qiao, Heteroatom-doped graphene-based materials for energy-relevant electrocatalytic processes, *ACS Catal.* 5 (2015) 5207–5234.
- [32] H.-J. Zhang, X. Zhang, S. Yao, H. Hu, Z.-F. Ma, J. Yang, Simultaneous doping of nitrogen and fluorine into carbon (NFC) as metal-free oxygen reduction electrocatalysts, *J. Electrochem. Soc.* 164 (2017) H1081–H1085.
- [33] Y. Lv, L. Yang, D. Cao, Sulfur, nitrogen and fluorine triple-doped metal-free carbon electrocatalysts for the oxygen reduction reaction, *ChemElectroChem* 6 (2019) 741–747.
- [34] S. Hong, S. Park, Electrochemical preparation and characterization of poly (1, 5-diaminonaphthalene) as a functional polymer, *Electrochem. Soc* 150 (2003) E360–E365.
- [35] R. Ojani, J.-B. Raouf, S.R.H. Zavvarmahalleh, Electrocatalytic oxidation of methanol on carbon paste electrode modified by nickel ions dispersed into poly (1, 5-diaminonaphthalene) film, *Electrochim. Acta* 53 (2008) 2402–2407.
- [36] D. Liu, L. Fu, X. Huang, K. Liu, J. Li, H. Xie, H. Wang, Y. Tang, Influence of Iron source type on the electrocatalytic activity toward oxygen reduction reaction in Fe-N/C for Al-air batteries, *J. Electrochem. Soc.* 165 (2018) F662–F670.
- [37] Y. Zhan, F. Xie, H. Zhang, Z. Lin, J. Huang, W. Zhang, X. Sun, Y. Zhang, J. Chen, H. Meng, Non noble metal catalyst for oxygen reduction reaction and its characterization by simulated fuel cell test, *J. Electrochem. Soc.* 165 (2018) J3008–J3015.
- [38] F. Li, H. Shu, X. Liu, Z. Shi, P. Liang, X. Chen, Electrocatalytic activity and design principles of heteroatom-doped graphene catalysts for oxygen-reduction reaction, *J. Phys. Chem. C* 121 (2017) 14434–14442.
- [39] T. Gao, F. Zhou, W. Ma, H. Li, Metal-organic-framework derived carbon polyhedron and carbon nanotube hybrids as electrode for electrochemical supercapacitor and capacitive deionization, *Electrochim. Acta* 263 (2018) 85–93.
- [40] Y. Li, J. Qi, J. Li, J. Shen, Y. Liu, X. Sun, J. Shen, W. Han, L. Wang, Nitrogen-doped hollow mesoporous carbon spheres for efficient water desalination by capacitive deionization, *ACS Sustain. Chem. Eng.* 5 (2017) 6635–6644.
- [41] J. Liu, M. Lu, J. Yang, J. Cheng, W. Cai, Capacitive desalination of ZnO/activated carbon asymmetric capacitor and mechanism analysis, *Electrochim. Acta* 151 (2015) 312–318.
- [42] T.X.H. Le, R. Esmilaire, M. Drobek, M. Bechelany, C. Vallicari, S. Cerneaux, A. Julbe, M. Cretin, Nitrogen-doped graphitized carbon electrodes for bioelectrochemical pollutant removal, *J. Phys. Chem. C* 121 (2017) 15188–15197.
- [43] F. Zheng, Y. Yang, Q. Chen, High lithium anodic performance of highly nitrogen-doped porous carbon prepared from a metal-organic framework, *Nat. Commun.* 5 (2014) 5261.